Brief Review

LASER COOLING AND TRAPPING OF ATOMIC STRONTIUM FOR ULTRACOLD ATOMS PHYSICS, HIGH-PRECISION SPECTROSCOPY AND QUANTUM SENSORS

F. SORRENTINO, G. FERRARI, N. POLI, R. DRULLINGER* and G. M. TINO†

Dipartimento di Fisica and LENS — Università di Firenze, INFN, INFM, I-50019 Sesto Fiorentino (FI), Italy

†*guglielmo.tino@fi.infn.it*

Received 19 June 2006

This review describes the production of atomic strontium samples at ultra-low temperature and at high phase-space density, and their possible use for physical studies and applications. We describe the process of loading a magneto-optical trap from an atomic beam and preparing the sample for high precision measurements. Particular emphasis is given to the applications of ultracold Sr samples, spanning from optical frequency metrology to force sensing at micrometer scale.

Keywords: Laser cooling; ultracold atomic physics; quantum degenerate gases; quantum sensors; matterwave interferometry; inertial sensors; optical metrology; ultrastable lasers.

1. Introduction

Recently, laser-cooled atomic strontium has been the subject of active research in several fields spanning from all-optical cooling towards quantum degeneracy for bosonic,[1,2] and fermionic[3] isotopes, cooling physics,[4,5] continuous atom laser,[6] detection of ultra-narrow transitions,[7–10] multiple scattering,[11] and collisional theory.[12]

Much of that interest relies on the features of the electronic level structure of alkali-earth atoms, that make them ideal systems for laser manipulation and for the realization of quantum devices. Among the alkali-earth metals, strontium summarizes most of the useful properties both for the preparation of ultracold samples and for applications.

The ground-state Sr atom presents a strong and quasi-closed optical transition well suited for efficient trapping in magneto-optical traps (MOT's) from thermal samples,[13,14] and a multiplet of weak intercombination transitions with large interest in laser cooling and optical metrology. All of these transitions are easily accessible with compact solid-state laser sources, as described in Appendix A. Second-stage

*On leave from NIST, 325 Broadway, Boulder, Colorado 80305, USA.

cooling on the narrow $^1S_0$-$^3P_1$ intercombination line was proven to be an efficient method to reduce the sample temperature down to the photon recoil limit.[1]

The absence of a nuclear spin in all of the bosonic isotopes greatly simplifies the electronic energy spectrum with respect to the already simple structure of alkali atoms, and allows a direct verification of theories in the field of light scattering[15] and laser cooling.[5] Moreover, the lack of nuclear spin results in minimum sensitivity to stray magnetic fields: this has important consequences on high-precision measurements, as discussed in Secs. 6 and 7.

Interatomic collisions may represent an important source of perturbations in atomic quantum devices. In this respect, the ^{88}Sr atom exhibits excellent features due to its remarkably small collisional cross-section, resulting in the longest coherence time for Bloch oscillations observed so far.[16]

As a consequence of their zero magnetic moment, ground-state bosonic Sr isotopes cannot be magnetically trapped. However, optical dipole trapping with far-off resonant laser fields provides an effective method for trapping in conservative potentials. By properly choosing the wavelength of the trapping laser field, it is possible to design optical potentials that shift equally levels belonging to the singlet and triplet manifolds, hence avoiding perturbations to a given intercombination line.[17] This feature is the basis of laser cooling in dipole traps and allows one to reach a temperature close to the recoil limit with a phase-space density close to quantum degeneracy both with bosonic and fermionic isotopes.[2,3,18]

Several groups are presently working on laser cooled strontium. The Tokyo group first demonstrated the double-stage optical cooling down to sub-μK temperatures;[1] they also proposed and realized a Sr "optical lattice clock",[19] and made pioneering studies on electric microtraps for strontium.[20] The JILA group has made interesting studies on cooling physics,[4,5] and on metrological applications.[10] Our group is concerned both with ultracold physics studies,[2] and with applications to optical metrology[9] and quantum devices.[16] The BNM-SYRTE group is mainly concerned with metrological applications,[8,21,22] the Houston group with ultracold Sr physics,[23,24] while the Nice group has studied multiple scattering of light from cold Sr samples,[15] and analyzed several details of the Sr cooling mechanisms.[25]

From the experimental point of view, some of the techniques and solutions involved in atomic strontium cooling are specific to this atom and to some extent uncommon in the field of atomic physics and laser cooling. In this paper we give a detailed description of how to prepare an ultra-cold strontium sample which is well suited for high-precision spectroscopy, the study of quantum degenerate gases and quantum sensors. The presentation has the following structure:

- Sec. 2 summarizes the properties of the strontium atom,
- Sec. 3 describes the process of laser cooling of strontium starting from the slowing of a thermal beam, to the cooling down to the photon recoil limit and trapping in a conservative potential,
- Sec. 4 deals with the study of ultracold collisions on the ground-state bosonic Sr isotopes,

Table 1. Natural Sr isotopes (NIST data).

Isotope	Relative atomic mass	Relative abundance	Nuclear spin
^{88}Sr	87.905 6143(24)	82.58(1)%	0
^{86}Sr	85.909 2624(24)	9.86(1)%	0
^{87}Sr	86.908 8793(24)	7.00(1)%	9/2
^{84}Sr	83.913 425(4)	0.56(1)%	0

- in Sec. 5 we show some recent advances towards the realization of a Bose–Einstein condensate (BEC) of strontium,
- in Sec. 6 we present the use of ultracold Sr atoms as force sensors at micrometric scale,
- in Sec. 7 we review the recent frequency measurements on the Sr intercombination transitions with application to optical metrology,
- in Appendix A we give a detailed description of the experimental setup employed in laser cooling of strontium, namely the vacuum apparatus and the laser sources.

2. Properties of the Strontium Atom

The main properties of atomic strontium are common to almost all alkaline-earth metals. At ambient temperature it appears as a metal. Its vapor pressure is quite low, and it reaches 1 mTorr at 1000 Kelvin. The Sr atom is rather reactive: it forms compounds with oxygen, nitrogen, water and silicates, while it is inert against sapphire. Thus in working with Sr vapors it is common to employ sapphire windows.[109]

Strontium has four natural isotopes, whose properties are listed in Table 1. The bosonic (even) isotopes have zero nuclear spin, thus they are perfect scalar particles in the $J = 0$ states. This has important consequences for applications to optical metrology and quantum sensors (see Secs. 6 and 7).

Concerning the electronic level structure, due to the presence of two electrons in the outer shell the atomic states can be grouped into two separate classes: singlets and triplets. Since the spin-orbit interaction breaks the spin symmetry, intercombination transitions between singlet and triplet states are weakly allowed.[26] A simplified scheme of relevant Sr levels and transitions is shown in Fig. 1.

The strong ^{1}S$_0$-^{1}P$_1$ transition at 461 nm has a natural width of 32 MHz, and it is used for laser cooling and trapping.[13,14] Such transition is not perfectly closed, due to a small leakage towards the 4d ^{1}D$_2$ state (branching ratio $\sim 10^{-5}$). The direct ^{1}D$_2$-^{1}S$_0$ decay channel is forbidden in dipole approximation, and atoms from the ^{1}D$_2$ basically decay towards the 5p ^{3}P$_2$ (branching ratio 33%) and 5p ^{3}P$_1$ (branching ratio 67%) states.

The line strength of the three 5s^2 ^{1}S-5s5p ^{3}P intercombination transitions range from the relatively high value (7.6 kHz) of the 689 nm ^{1}S$_0$-^{3}P$_1$ line to the virtually zero value of the ^{1}S$_0$-^{1}P$_0$ line for the even isotopes in the absence of external fields. In ^{87}Sr the 0-0 line has a natural linewidth of ~ 1 mHz due to hyperfine mixing.

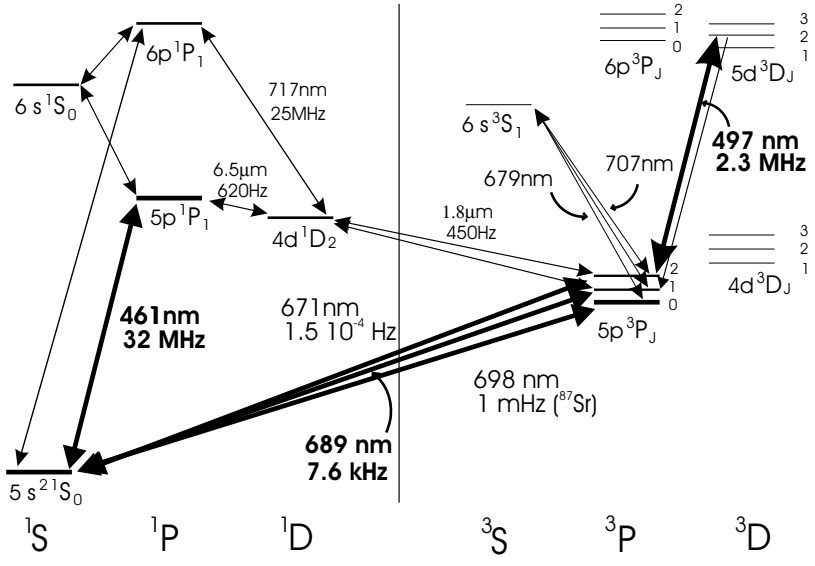

Fig. 1. Electronic level structure of atomic strontium. The transitions relevant for laser cooling and optical manipulation are indicated as well as their linewidths.

3. Laser Cooling and Trapping

A magneto-optical trap operated on the $^1S_0$-$^1P_1$ line requires the use of a blue laser source, that can be realized through second-harmonic generation from a semiconductor laser, as described in Appendix A.2.

The final temperature in such a "blue MOT" is limited to few mK by the linewidth of the $^1S_0$-$^1P_1$ transition: the ground state of alkaline-earth even isotopes has no hyperfine or Zeeman structure, and this prevents the application of sub-Doppler cooling techniques. However, the presence of narrow intercombination transitions allows efficient second-stage Doppler cooling down to sub-recoil temperatures, as described in Sec. 3.4. In ^{87}Sr, the ground-state hyperfine structure offers the chance for sub-Doppler cooling on the $^1S_0$-$^1P_1$ transition, as demonstrated by the JILA group.[4] Alternatively, it is possible to apply sub-Doppler cooling techniques to atoms trapped in the metastable $^3P_2$ level, as already demonstrated on Ca.[27]

In this section we illustrate the Sr cooling and trapping in detail, as performed in our laboratory. We start by preparing a mK sample in the blue MOT from a Zeeman-slowed atomic beam, using optical pumping to recycle atoms from the metastable $^3P_2$ level. Then we transfer the atoms to a "red MOT" operated on the $^1S_0$-$^3P_1$ intercombination line, where we cool them down to μK temperatures. Our apparatus allows us to trap different Sr isotopes simultaneously, as described in Sec. 3.5. The final step consists in loading an optical dipole trap.

3.1. *Zeeman slowing and atomic beam collimation*

The sequence for cooling and trapping on the 461 nm resonance line follows standard techniques, as already reported by other groups.[1,4,14,28] We slow the thermal atomic beam to few tens of m/s in a 30-cm long Zeeman-slower[29] based on a two-stages tapered coil with a zero crossing magnetic field, and a counter-propagating laser beam frequency shifted by 480 MHz to the red of the $^1S_0$-$^1P_1$ transition. The beam, with typical power of 40 mW, has a 7 mm $1/e^2$ radius at the MOT and it is focused on the capillaries (see Appendix A.1). The distance between the capillaries of the oven and the MOT region is 100 cm.

The atomic beam brightness can be increased with a 2-D transverse cooling stage before the Zeeman slower.[30,31] This improves the MOT loading both by increasing the atomic flux coupled into the differential pumping tube (see Appendix A.1), and by effectively reducing the final diameter of the atomic beam after the Zeeman slower.

We implement a 2D optical molasses with two 461 nm beams sent perpendicularly to the atomic beam, in multipass geometry on two orthogonal planes. The beams are red detuned by 20 MHz with respect to the $^1S_0$-$^1P_1$ resonance. At given optical power, the multi-pass geometry improves the transverse cooling efficiency by increasing the length of the interaction region. In the present setup we use beams with $1/e^2$ diameter of 2.5 mm^2 bouncing about 12 times to cover an interaction length of 4 cm. The interaction starts 15 cm after the capillaries (see Appendix A.1). In that region the beam diameter has already reached about 11 mm.

Without beam collimation we can couple into the differential pumping tube (placed 24 cm far from collimation region) about 10% of the total atomic flux. With the 2D molasses we increase the coupling by a factor of 4 in optimal conditions (laser detuning $\sim$ 20 MHz, optical power $\sim$ 20 mW). This simple scheme can also be used to deflect the atomic beam.

3.2. *Blue MOT*

The slowed atoms are then cooled and trapped in a MOT operated on the $^1S_0$-$^1P_1$ transition 40 MHz to the red with respect to resonance. Three retro-reflected beams with a 5 mm $1/e^2$ radius cross in the MOT region with almost mutually orthogonal directions. The vertical beam is collinear with the magnetic quadrupole axis of an anti-Helmholz pair of coils. The field gradient at the quadrupole center is 50 Gauss/cm. Taking into account the coupling efficiency of the blue laser source into the fiber (70%) and the efficiency of the AOMs ($75 \div 80\%$), the remaining 120 mW are split into the three channels: typical power values are respectively 60 mW for MOT beams, 40 mW for Zeeman slower and 20 mW for transverse cooling beams. The total 461 nm light incident on the MOT region amounts to $\sim$ 90 mW/cm^2.

We have a rough estimate of the number of trapped atoms by collecting the 461 nm fluorescence on a calibrated photodiode. By changing the blue laser detuning

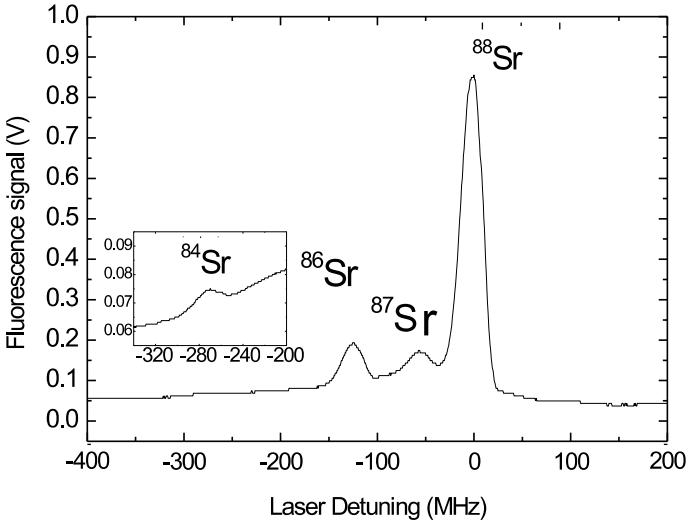

Fig. 2. Fluorescence of blue MOT as a function of laser detuning. Resonances corresponding to the different isotopes are visible.

we are able to separately trap the four natural Sr isotopes, as shown in Fig. 2. For a more accurate measure of the atom number we perform absorption imaging on a CCD with a resonant 461 nm horizontally propagating probe beam. We measure the sample temperature with standard time-of-flight technique.

The lowest temperatures measured in the blue MOT are typically higher than the Doppler limit by at least a factor two. The Nice group has shown that the extra-heating mechanisms causing such discrepancy can be explained in terms of intensity fluctuations in the MOT laser beams.[25]

3.3. *Optical repumping from metastable states*

The $^1S_0$-$^1P_1$ transition used in the first stages of cooling and trapping is not perfectly closed due to the decay channel of the $5s5p\,^1P_1$ towards the $5s4d\,^1D_2$ state, that has a branching ratio of 2×10^{-5}. Atoms in the latter state may decay back to the ground state through the $5s5p\,^3P_1$ within less than 1 ms, or may decay to the metastable $5s5p\,^3P_2$ and be lost (see Fig. 1). Under typical MOT conditions this process limits the MOT lifetime to few tens of milliseconds.

Some groups already circumvented this limitation by optical pumping atoms from the metastable $5s5p\,^3P_2$ to the ground state via the $5s6s\,^3S_1$ state with 707 nm light.[32] Since the $5s6s\,^3S_1$ state is also coupled to the metastable $5s5p\,^3P_0$ an additional laser at 679 nm is necessary in this scheme. To reduce the number of repumping lasers we use a different approach which involves the $5s5d\,^3D_2$ state and requires one single laser at 497 nm. Concerning the optical pumping, the $^3D_2$ state is coupled basically to the $^3P_2$ and $^3P_1$ states, then efficient pumping is insured within few absorption cycles. To this purpose during the loading we illuminate the blue MOT with light at 497 nm, produced by the source described in

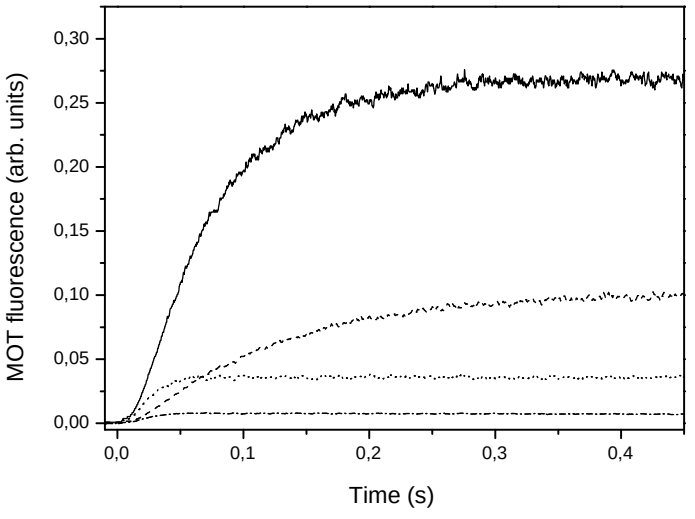

Fig. 3. Fluorescence of the charging MOT. Solid line: with transverse cooling and repumper. Dash: with repumper. Dot: with transverse cooling. Dash-dot: without repumper or transverse cooling.

Appendix A.2, which is kept on resonance with the repumping transition. Figure 3 shows the effect of the repumping field on the ^{88}Sr MOT loading in different conditions. Without the repumper the MOT loading time ($1/e$) is 10.2 ms regardless to the presence of the atomic beam transverse cooling, and correspondingly to the flux of atoms captured. In presence of the repumper we observe a 0.24 s lifetime when few atoms are present in the MOT, and a decreasing lifetime down to 0.11 s at full MOT charging. This reduction in lifetime is explained in terms of light assisted collision.[32]

Due to the difference in the natural isotope abundance (see Sec. 2), the loading flux into the MOT varies correspondingly. In typical conditions, i.e. when operating with the transverse cooling and optical repumping from the metastable state, and with the Sr oven kept at ~ 700 K, the steady-state blue MOT population amounts to $\sim 10^8$ atoms for ^{88}Sr and $\sim 10^7$ atoms for ^{86}Sr.

3.4. *Red MOT*

The Tokyo group first realized a strontium MOT operated on the $^1S_0$-$^3P_1$ line.[1] Such system has been exhaustively studied by the JILA group, both theoretically and experimentally.[5] The dynamics of laser cooling on narrow transitions presents several interesting features. Unlike in the case of ordinary magneto-optical traps, for the $^1S_0$-$^3P_1$ transition in alkaline-earth atoms the natural linewidth Γ is of the order of the recoil frequency shift Γ_R. In such conditions both mechanical and thermodynamical MOT properties cannot be explained by the ordinary semiclassical Doppler theory of laser cooling. In particular, the role of gravity becomes non

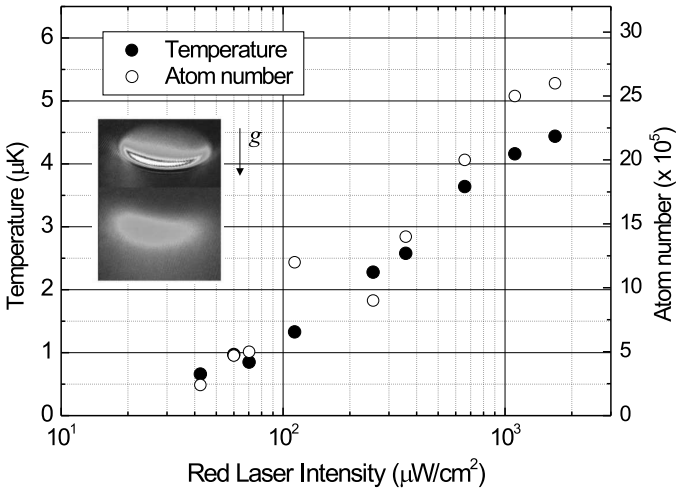

Fig. 4. Measured atomic temperature and population of the red MOT as a function of the laser intensity with our apparatus. The inset shows *in-situ* and free-fall images of the trapped atoms.

negligible, and the atomic temperature can be lower than the recoil limit $T_R = \frac{\hbar\Gamma_R}{k_B}$.

When the laser detuning δ is negative and larger than the power-broadened linewidth $\Gamma\sqrt{1+\frac{I}{I_{sat}}}$, the atoms interact with the MOT laser beams only on a thin ellipsoidal shell, corresponding to the surface where the laser frequency offset compensates for the Zeeman shift. The maximum radiation force is only one order of magnitude larger than gravity. As a result, the atoms sag on the bottom of the ellipsoid, as shown in the inset of Fig. 4. In such conditions the atomic temperature is mainly determined by the interaction with the upward propagating vertical MOT beam. With typical laser intensities of $I \simeq 10^1 \div 10^4 I_{sat}$, measured temperatures are in good agreement with a semiclassical model, and can be expressed as

$$T = \frac{\hbar\Gamma\sqrt{1+\frac{I}{I_{sat}}}}{2k_B}, \tag{1}$$

which is lower than the Doppler temperature at the same detuning. At low laser intensity ($I \approx I_{sat}$), the cooling mechanism becomes fully quantum-mechanical, and the minimal attainable temperature is $\frac{T_R}{2}$.[5] Figure 4 shows the dependence of the MOT temperature on the 689 nm laser intensity, as measured in our laboratory.

The JILA group also studied the case of positive laser detuning, revealing the appearance of novel striking phenomena such as momentum-space crystals. They showed that driving the atomic system with 689 nm light blue detuned from the $^1S_0$-$^3P_1$ resonance may result in a periodic pattern in the atomic velocity distribution.[5]

Second-stage cooling of the odd Sr isotope is more complex, due to the hyperfine structure of both ground and excited states. The Tokyo group has shown that using

two lasers at 689 nm it is possible to cool and trap ^{87}Sr atoms at phase-space densities close to the Fermi degeneracy.[33]

We here illustrate the red MOT for bosonic Sr isotopes as realized in our laboratory. The 689 nm light for the MOT beam (14 mW) is provided by a slave laser injection-locked with light coming from the stable master laser described in Appendix A.3. The beam spot is then enlarged to the same radius as the 461 nm MOT beams and overlapped to the blue beams with a dichroic mirror. After that mirror, the two wavelengths share the same broad-band optics: polarizing beam splitters, mirrors and waveplates.

The linewidth of the intercombination transition is not sufficient to cover the Doppler broadening corresponding to the velocity distribution of the sample trapped in the blue MOT. An efficient solution consists in broadening the spectrum of the 689 nm laser field.[1] On the contrary, groups working on other alkaline-earth atoms (i.e. Ca and Mg) employ a resonant coupling to some higher level to quench the ^{3}P$_1$ lifetime,[34] thus increasing the effective strength of the intercombination transition, as the maximum radiation force would be otherwise lower than gravity.

We add a frequency modulation at 50 kHz in the first 200 ms. The total frequency span is 2 MHz, corresponding to 40 sidebands, with an intensity of 120 μW/cm^2 per sideband (the saturation intensity is $I_{sat} = 3$ μW/cm^2). The central frequency is red detuned by 1 MHz with respect to resonance. At the end of the FM recapture, we normally obtain a cloud at a temperature of about 20 μK. After that we remove the frequency modulation, set a fixed red detuning from ^{1}S$_0$-^{3}P$_1$ transition and reduce the beam intensity in the last 60 ms of cooling. Working at 350 kHz below resonance and reducing the total light intensity on the MOT to 70 μW/cm^2, we can then transfer about 10% of the atoms from the blue MOT to the red MOT at temperatures below 1 μK.

3.5. *Cooling and trapping isotopic mixtures*

Among the experiments on ultracold atoms, much work is being concentrated on the study of mixtures of different atomic species[35,36,110] or different isotopes of the same species.[40,38,39,37] Mixtures offer a way to exploit collisional physics not applicable in single species samples.[41] They also offer additional degrees of freedom, such as sympathetic cooling, in order to achieve the degenerate quantum regime with atoms for which evaporative cooling is not efficient.[42]

For simultaneous trapping of different isotopes previous experiments employed laser sources delivering the necessary frequency components for each isotope involved.[40,43] In the case of the strontium blue MOT, this approach may be difficult to apply because of the complexity of the laser sources and the limited laser power. An alterative solution is presented by the use of the magnetically trapped ^{3}P$_2$ state as a dark atom reservoir.[44–46] During the blue MOT phase without the repumper, the small loss channel of the excited ^{1}P$_1$ state towards the metastable ^{3}P$_2$ state provides a continuous loading of atoms into the potential given by the MOT's

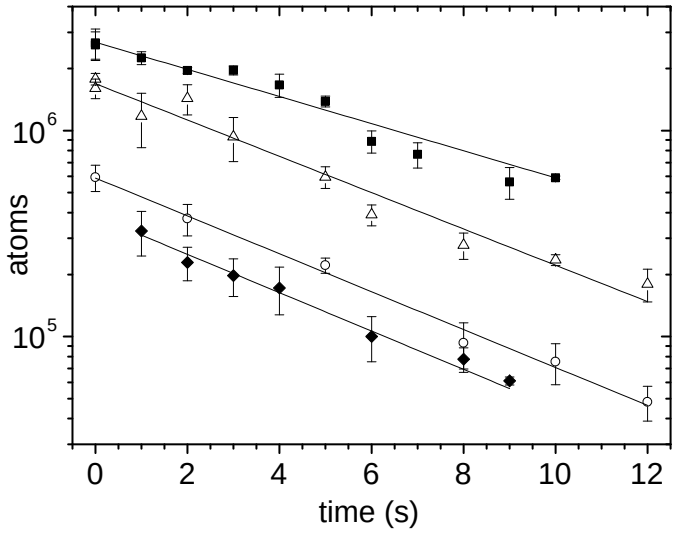

Fig. 5. Decay of the $^3P_2$ state when trapped in a 56 G/cm magnetic quadrupole. Circles (^{86}Sr) and squares ^{88}Sr refer to data taken for the individual isotopes with the blue MOT switched off; diamonds (^{86}Sr) and triangles (^{88}Sr) with the blue MOT operating on the undetected isotope. The measurements are taken after red MOT recapture. Reprinted figure with permission from N. Poli *et al.*, *Phys. Rev. A* **71** (2005) 061403(R). Copyright (2005) by the American Physical Society.

magnetic quadrupole. Figure 5 reports our lifetime measurements on the magnetically trapped metastable isotopes. By using the same blue laser source, one can sequentially load different isotopes into the magnetic potential by just stepping the laser frequency to the different resonances.

We typically start by collecting one isotope (say ^{86}Sr) for a few seconds, then we tune the blue laser on resonance to the other isotope (say ^{88}Sr). Once the isotopic mixture is prepared in the $^3P_2$ state, the blue light is switched off, and the FM red MOT is switched on as well as the repumping beam. The isotopic shift on the repumping transition is smaller than the resonance width of the $^3P_2$-$^3D_2$ transition observed on the blue MOT fluorescence, which results in efficient, simultaneous optical pumping of ^{88}Sr and ^{86}Sr on a time scale short with respect to the red MOT capture time. The loading of a single isotope into the magnetic potential was already described by Nagel *et al.*,[45] and we did not observe significant differences in the behavior when loading two isotopes. Figure 5 shows the measurement of the lifetime for each isotope, both when individually trapped and in the presence of the blue MOT working on the other isotope. The measured lifetime values are all of the order of 5 s, close to the background pressure limited lifetime of 7 s.

The laser source for the operation of the two-isotope red MOT is composed of two slave lasers injected from the same frequency stabilized master with a frequency offset corresponding to the isotopic shift of 163 817.3 kHz.[9] Subsequently, the frequency and intensity of the two beams are controlled by double pass AOMs

driven by the same RF, the beams are superimposed on a polarizing beam splitter, and then they are overlapped to the blue MOT beams as described previously. Comparing the two-isotope red MOT with the single isotope one, with the same atom numbers we do not observe any effect in the transfer efficiency and final temperature due to the presence of the second isotope. In this way, we obtain samples with up to 10^7 (10^6) atoms of ^{88}Sr (^{86}Sr) at a temperature 2 μK (1 μK). We attribute the difference in the loading to the natural abundances and to minor differences in the red MOT parameters. By varying the order of loading and the loading times of the two isotopes we can vary almost arbitrarily the final ratio of populations.

The atom number and temperature are measured independently on the two isotopes by absorption imaging with the resonant 461 nm probe beam, and the contribution of the non-resonant isotope is taken into account.

3.6. *Optical dipole trap*

In magneto-optical traps the atomic temperature and lifetime are fundamentally limited by resonant photon scattering and light-assisted collisions. In all experiments requiring long storage times or ultra-low temperatures, it is convenient to transfer the atoms into a conservative trap. The ground-state even isotopes of alkaline-earth atoms cannot be magnetically trapped, due to the absence of Zeeman structure. Though the Tokyo group has recently demostrated a clever scheme for Sr trapping with AC elecric fields,[20] in most cases the best choice consists in optical dipole traps. Moreover on two-electrons atoms it is possible to apply light-shift cancellation techniques to the intercombination transitions,[17] opening the way to optical spectroscopy with ultimate accuracy. However, the optical dipole trap is widely employed with magnetic atoms as well,[47] since it generally produces a stronger confinement than magnetic traps, up to the Lamb–Dicke regime in optical lattices,[48] and permits trapping in all the magnetic sub-levels.

In an optical dipole trap the confining force originates from the energy level gradient produced by the intensity-dependent light shift. The energy level shift ΔE of an atom in an optical field is proportional to the light intensity I and, in the rotating-wave approximation, inversely proportional to the frequency detuning δ from resonance:

$$\Delta E = \frac{\hbar \Gamma^2 I}{8 \delta I_{sat}}\,, \tag{2}$$

where Γ and I_{sat} are the linewidth and the saturation intensity of the resonance transition, respectively, while the photon scattering rate R_S scales as the light intensity and the inverse square of the laser detuning:

$$R_S = \frac{\Gamma^3 I}{4 \delta^2 I_{sat}}\,. \tag{3}$$

Thus, at a given trap potential depth, it is possible to reduce the heating due to photon scattering by increasing δ and I proportionally. In far-off resonant optical

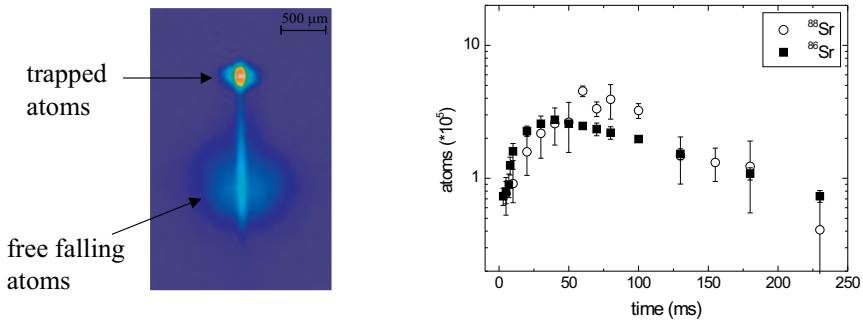

Fig. 6. Crossed-beams FORT loading. The inset shows an *in-situ* image of trapped atoms. The graph shows the measured FORT population as a function of the time overlap between FORT and red MOT. Reprinted figure with permission from N. Poli *et al.*, *Phys. Rev. A* **71** (2005) 061403(R). Copyright (2005) by the American Physical Society.

dipole traps (FORT) the effect of photon scattering is negligible for most practical purposes.

The trapping radiation couples singlet and triplet states independently. This results in a different dependence on the trapping wavelength for the light shift of the $^1S_0$ and $^3P_1$ levels, so that the differential shift vanishes at a "magic wavelength". This enables optical cooling into the dipole trap, since the detuning of the cooling radiation is not position-dependent.

For our optical dipole trap we employ the apparatus described in Appendix A.4. In most cases we use the horizontally propagating beam alone. This single-beam FORT has a trap depth of 90 μK. The computed radial and axial trap frequencies are $\omega_r = 2\pi \times 2$ kHz and $\omega_a = 2\pi \times 26$ Hz respectively. The vertical beam produces a maximum potential depth of about 12 μK. We find good agreement between computed and measured trap frequencies. The resonant 461 nm probe beam for time-of-flight absorption imaging propagates horizontally at an angle of about 30° with the horizontal FORT beam.

The transfer efficiency from the red MOT to the FORT results from a balance between loading flux and density dependent losses due to light assisted collisions.[17] Figure 6 shows typical loading curves, together with an in-situ image of the trapped atoms.

The AC Stark shift of the intercombination line depends on the direction of the FORT field with respect to the bias magnetic field **B**. We use the MOT quadrupole field to resolve the Zeeman structure of the $^1S_0$-$^3P_1$ line, and we keep the polarization of the FORT beam linear and orthogonal to **B**. In such conditions the resulting light shift is not critical for laser cooling in the FORT. The wavelength used for the dipole trap is only 7 nm away from the "magic wavelength" for the intercombination $^1S_0$-$^3P_1$ transition.[49] When the polarization of the dipole trapping light is orthogonal to the magnetic field the Stark shift for the $^1S_0$-$^3P_1$ transition is lower than 10 kHz. Thus, it is possible to cool the atoms while loading the dipole trap.[18]

4. Collisional Studies on Ground-State Even Sr Isotopes

The study of atomic collisions at low temperature has undergone a rapid development in recent years following the advent of a number of cooling techniques for dilute atomic gases. The measurement of collisional parameters gives insight into an interesting and promising physics, allowing tests of theoretical models for interatomic potentials and molecular wavefunctions.[32,50] Moreover, a precise knowledge of collisional properties is essential for experiments aiming to explore regimes of quantum degeneracy in atomic gases.[51,52]

Here we describe a systematic analysis on the ground-state collisional properties of the two most abundant bosonic Sr isotopes (^{88}Sr and ^{86}Sr) performed with our apparatus. More specifically, we evaluated the elastic cross-sections σ_{i-j} $(i, j = 86, 88)$ for both intra and inter-species collisions, and the three-body recombination coefficients K_i $(i = 86, 88)$ in the FORT. The elastic cross-sections were deduced by driving the system out of thermal equilibrium and measuring the thermalization rate together with the sample density. For the inelastic collisions, we measured the density dependence of the trap loss rate. The key point of our experimental procedure is a precise knowledge of the atomic density. This in turn requires a proper control of the trap frequencies. We assumed the equilibrium phase-space distribution in an ideal harmonic trap to infer the atomic density from the measured number of atoms N and temperature T. Our assumption is supported by the fact that the ratio $\eta = \frac{U}{k_B T}$ of trap depth and sample temperature was larger than 5 in all of our measurements. The equilibrium peak atomic density in a harmonic trap is

$$n_0 = N\bar{\nu}^3 \left(\frac{2\pi m}{k_B T}\right)^{\frac{3}{2}} \tag{4}$$

where $\bar{\nu}$ is the average trap frequency, m is the atomic mass and k_B is the Boltzmann constant. Our results show significant differences in the collisional properties of the two isotopes. Both the elastic cross-section and the three-body collision coefficient were found to be several orders of magnitude larger in ^{86}Sr than in ^{88}Sr, and the inter-species cross-section σ_{86-88} is much larger than the intra-species cross-section σ_{88-88}.

We adopted the standard technique of observing the cross-thermalization between orthogonal degrees of freedom.[53–56] The single-beam FORT geometry is not well suited for this experiment, as the temperature in the horizontal modes cannot be univocally determined with our apparatus, and because with ^{86}Sr in our experimental conditions the system turned out to be in hydrodinamic regime along the axial direction.[58,57] Given these constraints, we chose the crossed-beams geometry for the thermalization measurements.

In order to drive the system out of thermal equilibrium we performed a selective optical cooling along the vertical direction with resonant 689 nm light. For this purpose we took advantage of the fact that the FORT is located at the center of the red MOT, where atoms are not resonant with the horizontal MOT beams.[5]

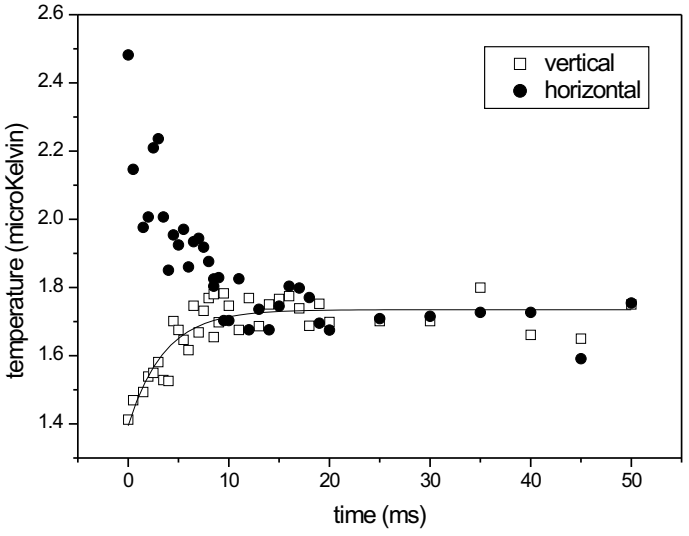

Fig. 7. Measurement of the thermalization rate for ^{86}Sr. The graph shows the temporal evolution of the horizontal and vertical temperatures after cooling on the vertical direction. The solid curve is an exponential fit to the vertical temperature data.

We chose the optical intensity and cooling time in such way to create a detectable thermal anisotropy without introducing dramatic losses.

We measured the intra-species thermalization rate τ_{th} by separately loading one isotope (either ^{88}Sr or ^{86}Sr) and observing the temporal evolution towards thermal equilibrium (see Fig. 7). In both cases the total trap loss rate was much lower than the thermalization rate, so the atom number was constant within shot-to-shot fluctuations.

We deduced the elastic cross-section from the measured thermalization rate, by assuming a value of 2.7 for the average number of collisions to reach thermalization, that is, $\tau_{th} = 2.7\tau_{coll}$.[53,54,59] The collision rate is given by

$$\frac{1}{\tau_{coll}} = \bar{n}\sigma\bar{v} \tag{5}$$

where $\bar{n}$ is the average atom density, $\bar{v}$ is the average relative velocity of colliding atoms, and σ is the cross-section. We computed $\bar{n}$ and $\bar{v}$ from the measured values for atom number N, average sample temperature T and average trap frequency $\bar{\nu}$. With our assumptions the average density is given by $\bar{n} = n_0/2\sqrt{2}$, while the average relative velocity is given by $\bar{v} = 4\sqrt{k_B T/\pi m}$.

We repeated our measurements for different values of the atom density, in order to check whether the observed cross-thermalization was due to elastic collisions or ergodic mixing between different degrees of freedom. The resulting values are $\sigma_{88-88} = 3(1) \times 10^{-13}$ cm^2 and $\sigma_{86-86} = 1.3(0.5) \times 10^{-10}$ cm^2. The uncertainty is mainly due to shot-to-shot fluctuations in the FORT population, that reflect in both density and temperature instabilities. Such results might be compared with

Table 2. Intra-species elastic cross-section for ^{88}Sr and ^{86}Sr, in cm^2.

Reference	σ_{88-88}	σ_{86-86}	Method
Tokyo group[60]	$3(1) \times 10^{-13}$		λ from PA spectra
Houston group[24]	$< 1.2 \times 10^{-13}$	$2.6 \times 10^{-10} < \sigma < 3.7 \times 10^{-9}$	λ from PA spectra
Our group[2]	$3(1) \times 10^{-13}$	$1.3(0.5) \times 10^{-10}$	cross-thermalization

the zero-temperature cross sections deduced from scattering length values through the relation $\sigma = 8\pi\lambda^2$, where λ is the s-wave scattering length. Scattering length values were obtained from photoassociation spectra by the Tokyo group for ^{88}Sr,[60] and by the Houston group for both isotopes.[24] As concerning σ_{88-88}, our value is consistent with the Tokyo work, while the Houston group predicts an even smaller cross-section. On the contrary, there is a fair agreement between our σ_{86-86} value and the Houston work. All of these results are summarized in Table 2.

We adopted a similar approach for the measurement of the inter-species cross sections.[61–64] The single-beam FORT was loaded with a mixture of ^{88}Sr (10^5 atoms) and ^{86}Sr (4×10^4 atoms). We then applied a selective optical cooling stage (duration 5 ms) to ^{88}Sr and observed the temperature evolution of the two samples (see Fig. 8). The ^{88}Sr is heated by ^{86}Sr to the equilibrium temperature in few tens of ms. For comparison, in absence of ^{86}Sr the temperature of ^{88}Sr grows by less than 5% in 100 ms. The resulting inter-species cross-section was found as $\sigma_{88-86} = 4(1) \times 10^{-12}$ cm^2. This value is significantly larger than the intra-species cross-section σ_{88-88}, suggesting the way to a novel and efficient sympathetic cooling mechanism.[2]

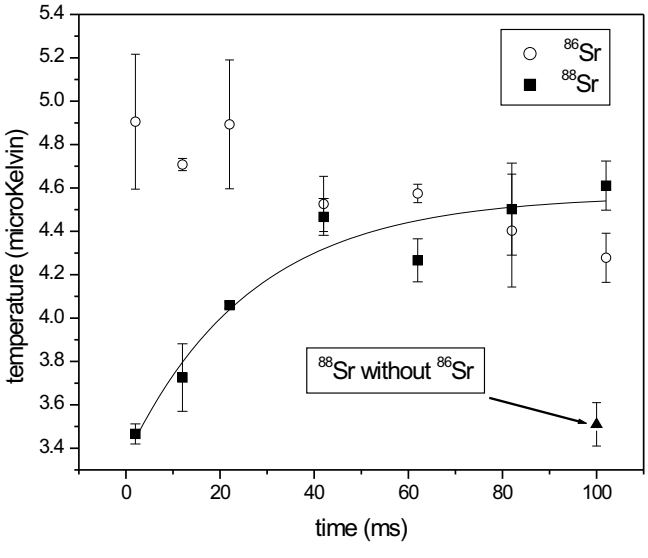

Fig. 8. Measurement of the interspecies thermalization rate. The graph shows the temperature evolution of ^{88}Sr and ^{86}Sr after selective cooling on ^{88}Sr. The solid curve is an exponential fit to the ^{88}Sr data. Trap populations are 10^5 atoms for ^{88}Sr and 4.5×10^4 atoms for ^{86}Sr.

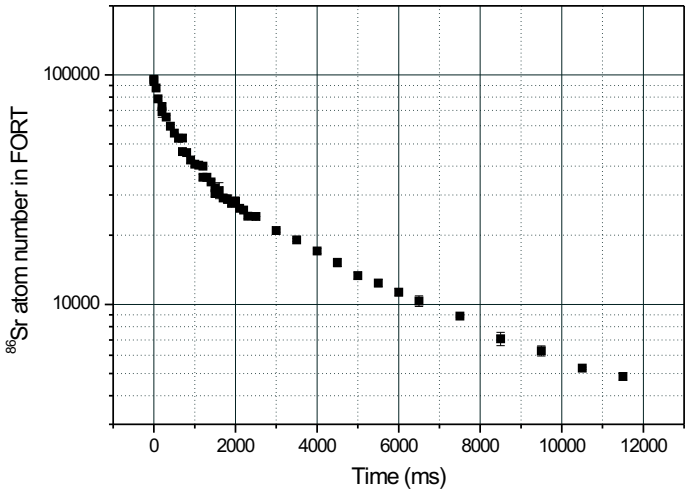

Fig. 9. Decay of trap population when loading ^{86}Sr atoms alone in the single-beam FORT. The sample temperature is 12 μK, trap depth is 90 μK.

We studied the inelastic collisions by loading a single isotope in the single-beam FORT (either ^{88}Sr or ^{86}Sr) and looking at the evolution of the number and temperature of trapped atoms in the FORT after the MOT operation was finished. We found no evidence for non-exponential decay with ^{88}Sr. The measured lifetime of 7 s is consistent with the residual background gas pressure of 10^{-8} torr. With the initial atom density at trap center of 3×10^{13} cm^{-3} this gives an upper limit of 10^{-27} cm^{6}s^{-1} for the K_{88} coefficient.

When loading the single-beam FORT with ^{86}Sr only, we observed a clear non-exponential decay (Fig. 9). We deduced the three-body recombination coefficient from the density dependence of the loss rate.[65] Integrating the loss rate equation

$$\dot{N} = -\Gamma_b N - K_{86} \int n^3(\mathbf{r}, t) d^3\mathbf{r} \tag{6}$$

where Γ_b is the linear loss rate for background gas collisions, with our assumptions we can write

$$\ln \frac{N}{N_0} = -\Gamma_b t - \frac{K_{86}(2\pi)^3 m^3 \bar{\nu}^6}{3^{\frac{3}{2}}} \int \frac{N^2(t)}{[k_B T(t)]^3} dt\,. \tag{7}$$

This formula is valid as long as additional losses due to evaporation can be neglected. In order to limit such effect, we select the coldest atoms by means of forced evaporation before the measurement.

We deduced the linear loss rate from the wing of Fig. 9. This value is consistent with the loss rate measured with ^{88}Sr. Then we performed a linear fit of $\ln \frac{N}{N_0} + \Gamma_b t$ versus $\int \frac{N^2(t)}{[k_B T(t)]^3} dt$ to derive the recombination constant. We repeated the measurement several times to average out density fluctuations reflecting in large uncertainty on K_{86}. The final result was $K_{86} = 1.0(0.5) \times 10^{-24}$ cm^{6}s^{-1}.

5. Towards a BEC of Strontium

Laser cooling is a very effective technique to reach phase-space densities within few orders of magnitude from quantum degeneracy. The limits in cooling at high density are set by the optical depth of the sample, i.e. reabsorption of scattered light, and light-assisted atom-atom collisions. Forced evaporative cooling represents the common way to circumvent these limits.[66] However, this procedure is not effective with all atoms. In particular, among the atoms cooled with optical methods, none of the alkali-earth atoms reached quantum degeneracy so far, except ytterbium which has an alkali-earth-like electronic structure.[67] A phase-space density of $\simeq 10^{-1}$ was reported for Sr but BEC could not be reached.[18]

On this respect, the results of the collisional measurements reported in Sec. 4 suggest that evaporative cooling on pure samples of either ^{86}Sr or ^{88}Sr cannot be very efficient in our experimental conditions. ^{86}Sr presents an extremely large elastic cross-section, a good point to establish a fast thermalization, but the 3-body recombination rate introduces a loss channel that is fatal with the typical geometries accessible through optical dipole trapping. An optical trap with a much larger trapping volume would partially suppress this loss channel.[68] ^{88}Sr instead turns out to be stable against 3-body decay, but the small elastic cross-section results in a long thermalization time compared to typical trap lifetime.

On the other hand, our results suggest a novel all-optical sympathetic cooling scheme.[2] In the isotope mixture the relatively large inter-species cross-section results in thermalization times typically of the order of few milliseconds. This thermalization is fast even on the time scale of laser cooling on the intercombination $^1S_0$-$^3P_1$ transition. Moreover, due to the 164 MHz ^{86}Sr-^{88}Sr isotopic shift and the natural linewidth of 7.6 kHz for the $^1S_0$-$^3P_1$ transition, laser cooling on one isotope has negligible effect on the other one. It is then possible to cool sympathetically a dense and optically thick cloud of one isotope (for instance ^{88}Sr) via optical cooling of a small sample of the other isotope (^{86}Sr). Continuous laser cooling of ^{86}Sr provides heat dissipation in the sample, while the small optical depth on ^{86}Sr does not limit the achievable minimum temperature. Sympathetic cooling with neutral atoms normally requires a thermal bath with heat capacity large with respect to that of the sample to be cooled. This is due to the fact that when the thermal bath is cooled by evaporative cooling, each lost atom carries an energy of the order of few times the temperature of the sample. In the case of optical-sympathetic cooling, each laser-cooled atom can subtract an energy of the order of the optical recoil in a time corresponding to a few lifetimes of the excited state, without being lost.

We implemented the optical-sympathetic cooling scheme by extending the temporal overlap between the FORT and the ^{86}Sr red MOT after switching off the ^{88}Sr MOT. Figure 10 reports the dynamics of optical-sympathetic cooling, starting from an initial temperature of 15-20 μK, limited by density dependent heating.[46,68] It can be observed that the cooling process does not induce losses on ^{88}Sr while the number of ^{86}Sr atoms exponentially decays with a 80 ms lifetime. About 100 ms

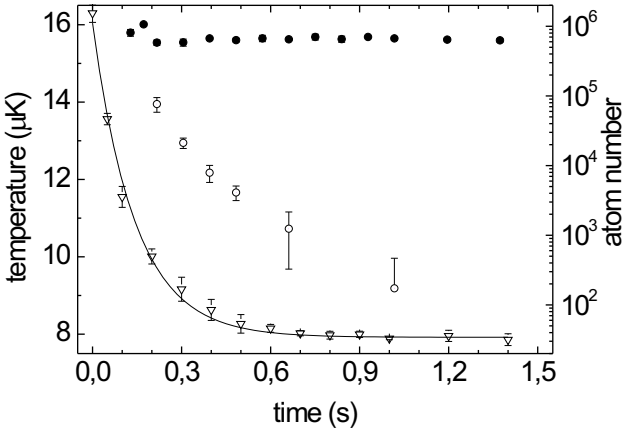

Fig. 10. Dynamics of an optically trapped ^{88}Sr cloud sympathetically cooled with laser cooled ^{86}Sr. Filled circles: ^{88}Sr atom number. Open circles: ^{86}Sr atom number. The number of ^{88}Sr atoms remains constant during the process, while ^{86}Sr decays exponentially with a 80 ms time constant. Under optimized conditions, the temperature (triangles) decreases with a 150 ms time constant and the mixture is always at thermal equilibrium. Reprinted figure with permission from G. Ferrari *et al.*, *Phys. Rev. A* **73** (2006) 023408. Copyright (2006) by the American Physical Society.

after switching off the ^{88}Sr red MOT, we observe that the mixture attains thermal equilibrium.

Under optimized conditions (overall optical intensity $100I_{sat}$) the temperature decays from the initial value with a 150 ms time constant. The minimum attainable temperature depends both on the intensity of the ^{86}Sr cooling beam, and the ^{88}Sr density. By keeping the cooling parameters on ^{86}Sr fixed at the optimum value and by varying the number of trapped ^{88}Sr, we determined the dependence of the final temperature on the ^{88}Sr density. For 6×10^5 ^{88}Sr atoms trapped in the FORT, the final temperature is 6.7 μK at a peak density of 1.3×10^{14} cm^3; the corresponding phase-space density is 5×10^{-2}. This value is only a factor of two lower than what was previously obtained without forced evaporation,[18] but it exhibits more favorable conditions for starting evaporative cooling, considering the higher spatial density (more than one order of magnitude higher) and the number of trapped atoms (gain $2 \div 10$).

Indeed we applied an evaporative cooling stage on ^{88}Sr by reducing the FORT intensity after the optical sympathetic cooling. This produced an increase in phase-space density by roughly a factor of 4, giving a maximum of 2×10^{-1}. Such result is consistent with a numerical simulation of forced evaporation in our experimental conditions. The gain in phase-space density during evaporative cooling is basically limited by the ^{88}Sr elastic cross-section. A promising way towards Bose–Einstein condensation seems to be the use of a dipole trap with variable geometry, to compensate for the reduction in thermalization rate during evaporation.[69]

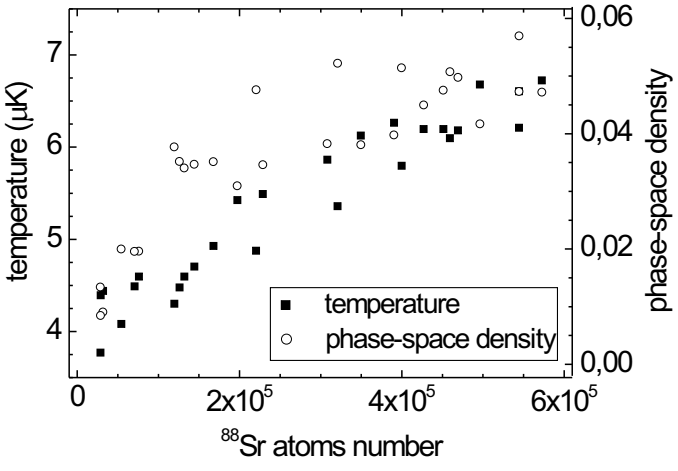

Fig. 11. Temperature and phase-space density of the ^{88}Sr cloud sympathetically cooled with laser cooled ^{86}Sr, as a function of the ^{88}Sr atom number. Reprinted figure with permission from G. Ferrari *et al.*, *Phys. Rev. A* **73** (2006) 023408. Copyright (2006) by the American Physical Society.

Figure 11 shows the dependence of ^{88}Sr temperature after the optical sympathetic cooling (without evaporative cooling) on the number of atoms in the trap. We determine the density-dependent heating $dT/dn \simeq 2\mu\text{K}/(10^{14}\ \text{cm}^{-3})$, which is 20 times lower than the equivalent value for pure laser cooled ^{88}Sr.[1] This large reduction is a direct consequence of the strong selectivity of the $^1\text{S}_0$-$^3\text{P}_1$ transition with respect to the two isotopes. The limit on the ^{86}Sr temperature of 4 μK for zero ^{88}Sr density can be attributed to the laser cooling dynamics in the tightly confining potential of the FORT.

6. Ultracold Sr Atoms as Quantum Sensors

Ultracold atomic strontium is particularly suited for applications in the field of quantum sensors. Atom interferometry has already been used with alkali-metals for precision inertial sensing,[70,71] for measuring fundamental constants,[72–74] and testing relativity.[75] The extremely small size of ultracold atomic samples enables precision measurements of forces at micrometer scale. This is a challenge in physics for studies of surfaces, Casimir effect,[76] and searches for deviations from Newtonian gravity predicted by theories beyond the standard model.[77–79]

An interesting class of quantum devices is represented by ultracold atoms confined in an optical lattice, that is a dipole trap created by a laser standing wave.[80] In particular, Bloch oscillations were predicted for electrons in a periodic crystal potential in presence of a static electric field[81] but could not be observed in natural crystals because of the scattering of electrons by the lattice defects. They were directly observed using atoms in an optical lattice.[82]

The combination of the periodic optical potential and a linear potential produced by a constant force F along the lattice wave-vector gives rise to Bloch oscillations at frequency ν_B given by $\nu_B = \frac{F\lambda_L}{2h}$, where λ_L is the wavelength of the light producing the lattice, and h is Plancks constant. Since λ_L is well known, the force along the lattice axis can be accurately determined by measuring the Bloch frequency ν_B. In order to perform a sensitive force measurement, a long coherence time with respect to the measurement duration is required. The most common effects limiting the coherence time for ultracold atoms are perturbations due to electromagnetic fields and atom-atom interactions. ^{88}Sr is in this respect an ideal choice because in the ground state it has zero orbital, spin and nuclear angular momentum. This makes it virtually insensitive to stray magnetic fields. In addition, as shown in Sec. 4 ^{88}Sr has remarkably small atom-atom interactions. Such properties make Sr in optical lattices a unique sensor for small-scale forces with better performances and reduced complexity compared to proposed schemes using degenerate Bose or Fermi gases.[83,84] This enables new experiments on gravity in unexplored regions.

We tested such idea by measuring the gravitational acceleration in our laboratory with a ^{88}Sr sample in a vertical optical lattice. To this end, we cool $\sim 5 \times 10^5$ atoms in the red MOT down to the recoil temperature (see Sec. 3.4), so that the vertical momentum distribution is narrower than the width of the first Brillouin zone.[81] Then we release the atoms from the MOT and we switch on adiabatically a one-dimensional optical lattice.

The lattice potential is originated by a single-mode frequency-doubled Nd:YVO_4 laser ($\lambda_L = 532$ nm) delivering up to 350 mW on the atoms with a beam waist of 200 μm. The beam is vertically aligned and retro-reflected by a mirror producing a standing wave with a period $\frac{\lambda_L}{2} = 266$ nm. The corresponding photon recoil energy is $E_R = \frac{h^2}{2m\lambda^2} = k_B \times 381$ nK. We populate about 100 lattice sites with 2×10^5 atoms at an average spatial density of $\sim 10^{11}$ cm^{-3}. We leave the atoms in the optical lattice for a variable time t, then we switch off the lattice adiabatically and we measure the momentum distribution of the sample by time-of-flight imaging, after a free fall of 12 ms.

We integrate along the horizontal direction the optical thickness obtained by absorption imaging. The resulting curve gives the vertical momentum distribution of the atomic sample: in Fig. 12 we show a typical plot after the integration.

We fit the measured momentum distribution with the sum of two Gaussian functions. From each fit we extract the vertical momentum center of the lower peak and the width of the atomic momentum distribution. We find that the latter is less sensitive against noise-induced perturbations to the vertical momentum. We can observe ~ 4000 Bloch oscillations in a time $t = 7$ s (see Fig. 13), with a damping time $\tau \sim 12$ s. To our knowledge, the present results for number of Bloch oscillations, duration, and the corresponding number of coherently transferred photon momenta, are by far the highest ever achieved experimentally in any physical system.

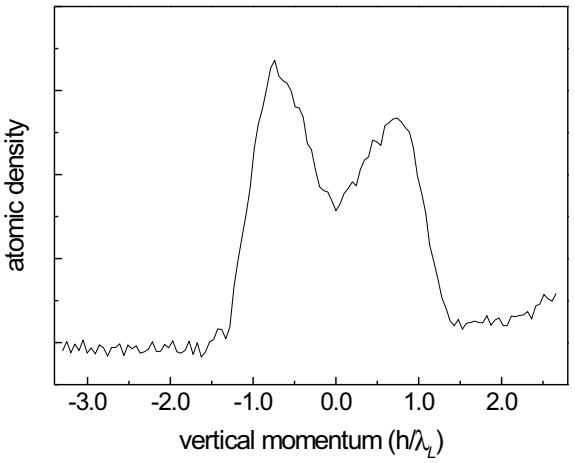

Fig. 12. Vertical momentum distribution of the atoms at the Bragg reflection.

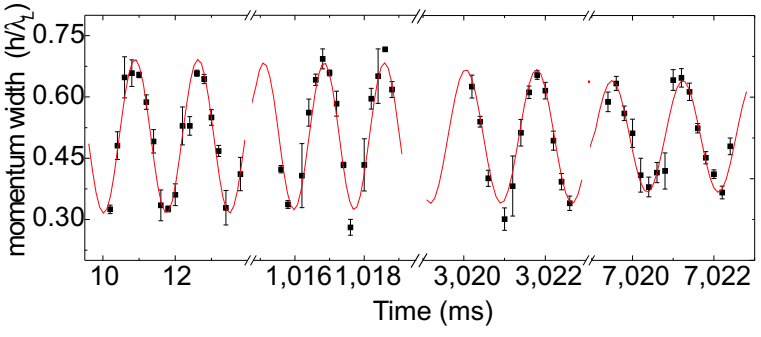

Fig. 13. Time evolution of the width of the atomic momentum distribution, showing Bloch oscillation of ^{88}Sr atoms in the vertical 1-dimensional optical lattice under the effect of gravity. From the data fit, a Bloch frequency $\nu_B = 574.568(3)$ Hz is obtained with a damping time $\tau \sim 12$ s for the oscillations.

From the measured Bloch frequency $\nu = 574.568(3)$ Hz we determine the gravity acceleration along the optical lattice $g_{meas} = 9.80012(5)$ ms^{-2}. The estimated sensitivity is $5 \times 10^{-6} g$. We expect that such precision may be increased by one order of magnitude by using a larger number of atoms, and reducing the initial temperature of the sample.

7. Frequency Measurements on the Sr Intercombination Lines

The advent of laser cooling techniques had important consequences on time-frequency metrology, by reducing the uncertainty on the frequency of atomic clocks caused by atom motion.

The recent progresses in two related fields, namely high-resolution laser spectroscopy and direct optical-frequency comb generation, opened the way to a new

generation of frequency standards based on transitions in the optical domain. The use of frequency combs based on self-mode-locked femtosecond lasers has made possible, for the first time, relatively simple optical-frequency measurements.[85,86] On the other hand, the realization of lasers with ultra-narrow emission band now enables spectroscopy on forbidden optical transitions with quality factor $Q = \frac{\nu}{\Delta\nu}$ in excess of 10^{15}.

Because of their higher frequency, optical transitions have the potential for greatly improved accuracy and stability compared to conventional atomic clocks based on microwave frequency transitions.[87] Different transitions are now considered as optical-frequency standards, involving single ions and neutral atoms.[88,89] While single ions offer an excellent control on systematic effects, clouds of laser cooled atoms have the potential for extremely high precision, as the large number of atoms reduces the quantum projection noise. Perhaps the use of optical lattices at the magic wavelength to confine neutral atoms in the Lamb–Dicke regime, as proposed for the first time on strontium,[17,90] summarizes the best of both worlds; that is, a large number of quantum absorbers with negligible shift of the optical clock transition due to external fields, Doppler effect and collisions.

Among the neutral atoms, Sr has long been considered as one of the most interesting candidates.[91] Several features, some of which are specific to this atom, allow different possibilities for the realization of a high precision optical clock. The visible intercombination 5^1S-5^3P lines from the ground state are easily accessible with semiconductor lasers. Depending on the specific fine-structure component and on the isotope, a wide choice of transitions with different natural linewidths is possible (see Sec. 2).

The first phase-coherent absolute frequency measurement of a Sr intercombination line was performed by our group on the 5^1S_0-5^3P_1 transition, using a thermal atomic beam.[9] This represented an improvement by several orders of magnitude with respect to previous data.[92] Our result is in agreement with subsequent phase-coherent measurements performed by the BNM-SYRTE group on a thermal sample,[8] and by the JILA group on a free-falling ultracold sample using a red MOT.[10] The JILA measurement provided a further improvement in the accuracy by more than two orders of magnitude.

However, the $^1S_0$-$^3P_1$ transition is not best suited as a final frequency reference, due to its natural linewidth of 7.6 kHz. Some groups recently began working on the 698 nm $^1S_0$-$^3P_0$ line, that is strictly forbidden in the even isotopes since it is a $J = 0 \rightarrow J = 0$ transition. In ^{87}Sr the hyperfine mixing enables direct $^1S_0$-$^3P_0$ excitation with a transition probability of ~ 1 mHz. The BNM-SYRTE group first measured such transition in a blue MOT with an uncertainty of 15 kHz.[8] The Tokyo group performed the first absolute frequency measurement in an optical lattice on this transition,[19] followed by the JILA and BNM-SYRTE groups.[22,93] All groups estimated an uncertainty ≤ 20 Hz for the absolute transition frequency. The corresponding 578 nm $^1S_0$-$^3P_0$ transition in Ytterbium was observed at NIST in a

~ 70 μK sample on the two odd isotopes, ^{171}Yb and ^{173}Yb, with an uncertainty of ~ 4 kHz.[94]

In spite of its large quality factor, the $^1S_0$-$^3P_0$ transition in odd Sr and Yb isotopes suffers from residual sensitivity to stray magnetic fields and optical lattice polarization, besides a complex line structure due to the presence of many magnetic sublevels. Several groups are now looking at the even Sr or Yb isotopes as the best candidates to represent optical frequency standards based on neutral atoms. Some groups have proposed different methods to directly excite the clock transition on the even Sr or Yb isotopes, by properly engineering the atomic level structure to create a finite and controllable $^1S_0$-$^3P_0$ transition probability. These methods basically consist in coupling the metastable $^3P_0$ level to other electronic states by using either multiple near-resonant laser fields,[95,96] or simply a small static magnetic field.[97] The latter scheme has been experimentally demonstrated on ^{174}Yb at NIST.[98] The possible instability due to site-to-site tunneling in optical lattice clocks has been addressed by the BNM-SYRTE group.[21] For accuracy goals at the 10^{-18} level they propose the use of vertical optical lattices, in order to lift the degeneracy between adjacent potential wells.

7.1. *Frequency measurement on the $^1S_0$-$^3P_1$ transition with a thermal beam*

In this section we discuss our precision frequency measurements on the intercombination 5^1S_0-5^3P_1 transition.[9] Using a femtosecond laser comb, we determined the absolute frequency of the transition for ^{88}Sr and ^{86}Sr and an accurate value for the isotope shift.

The frequency measurements have been performed through saturation spectroscopy on a thermal beam with the apparatus described in Appendix A.3. As frequency-comb generator we employed a commercial system based on a Kerr-lens mode-locked Ti:Sa laser with a repetition rate of 1 GHz.[99] Its repetition rate and carrier envelope offset frequency were locked to a GPS stabilized quartz oscillator. The strontium atomic beam is obtained from the metal heated to 830 K. Residual atomic beam divergency is 25 mrad and the typical atomic density in the detection region is 10^8 cm^{-3}. We derive a Doppler-free signal using a retro-reflected laser beam perpendicular to the atomic beam. The fluorescence light from the laser excited atoms is collected on a photomultiplier tube.

We estimate the indetermination on the reflection angle of the laser beam to be less than 10 μrad. The peak beam intensity of 60 μW/cm^2 (to be compared to the saturation intensity of 3 μW/cm^2) was chosen to obtain sufficient signal-to-noise for the RC lock onto the atomic resonance. A uniform magnetic field of 10 G (see Fig. 18) defines the quantization axis in the interrogation region such that the light is π polarized. The double pass AOM next to the atomic detection (AOM3) is frequency modulated at 10 kHz to derive the locking signal of the cavity onto the atomic line.

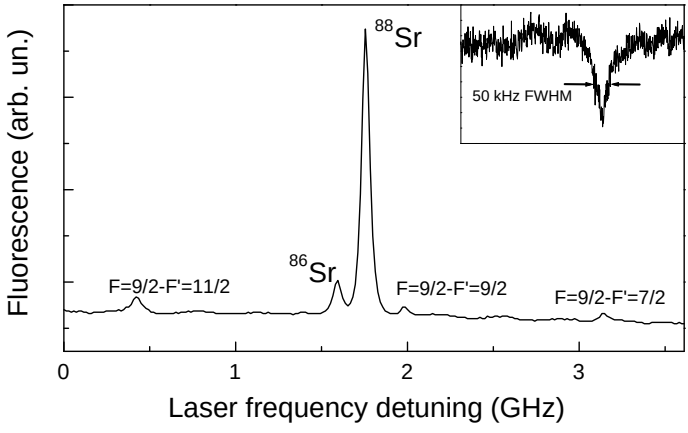

Fig. 14. Fluorescence spectrum of the strontium $^1S_0$-$^3P_1$ line at 689 nm. The lines of the two bosonic isotopes ^{86}Sr and ^{88}Sr, together with the hyperfine structure of the fermionic ^{87}Sr, can be resolved. The linewidth corresponds to the residual first order Doppler broadening in the thermal beam. Inset: sub-Doppler resonance of ^{88}Sr recorded by saturation spectroscopy using two counterpropagating laser beams. The amplitude of the dip is 10% of the Doppler signal. Reprinted figure with permission from G. Ferrari *et al.*, *Phys. Rev. Lett.* **91** (2003) 243002. Copyright (2006) by the American Physical Society.

Figure 14 shows the Doppler broadened resonances of ^{88}Sr, ^{86}Sr, and the hyperfine structure of ^{87}Sr. The residual atomic beam divergency produces a residual Doppler broadening of 60 MHz FWHM. In the inset, the sub-Doppler signal for ^{88}Sr is shown. Two independent measurements of the sub-Doppler resonance show a FWHM of about 50 kHz, which is in agreement with the expected value considering the saturation and transit time broadening, and the recoil splitting.

Figure 15 shows the result of the measurement of the ^{88}Sr transition frequency taken over a period of several days. Each data point corresponds to the averaging of the values resulting from consecutive measurements taken with a 1 s integration time over $100 \div 200$ s. The error bars correspond to the standard deviation for each data set. We evaluated first- and second-order Doppler and Zeeman effects, ac Stark shift, collisional shifts, and mechanical effects of light. The resulting value for the ^{88}Sr transition frequency, including the corrections discussed previously, is 434 829 121 311 (10) kHz, corresponding to a 1σ relative uncertainty of 2.3×10^{-11}.

7.2. *^{86}Sr-^{88}Sr isotopic shift measurement*

With a minor change in the apparatus, we locked simultaneously the frequency of two laser beams to the sub-Doppler signals of ^{86}Sr and ^{88}Sr. This system allowed us to measure the isotopic shift of the $^1S_0$-$^3P_1$ transition by counting the beat note between the two interrogating beams. For this purpose, the reference cavity is locked to the ^{88}Sr resonance as described previously and the light for ^{86}Sr is derived from the same laser beam and brought to resonance through AOMs. The two beams

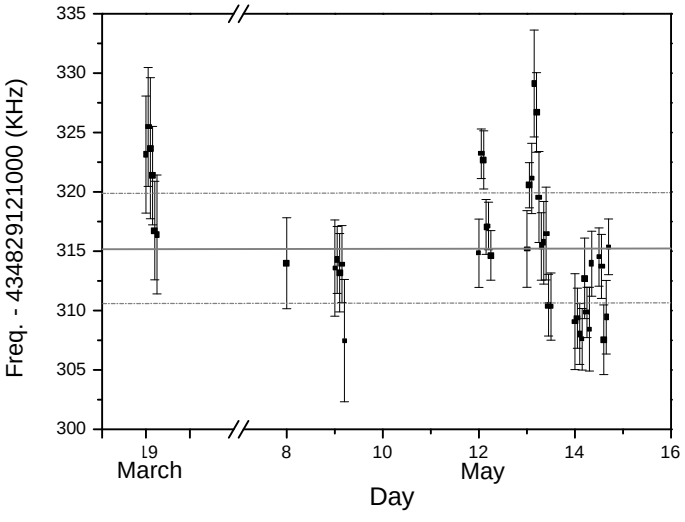

Fig. 15. Chronological plot of the optical frequency measurements. The error bars correspond to the standard deviation for each data set. Reprinted figure with permission from G. Ferrari *et al.*, *Phys. Rev. Lett.* **91** (2003) 243002. Copyright (2006) by the American Physical Society.

are overlapped in a single mode optical fiber and sent to the interrogation region. By frequency modulating the beams at different rates and using phase sensitive detection we get the lock signal for both the isotopes from the same photomultiplier. In this isotope-shift measurement most of the noise sources are basically common mode and rejected. The measured ^{88}Sr-^{86}Sr isotope shift for the $^1S_0$-$^3P_1$ transition is 163 817.4 (0.2) kHz. This value represented an improvement in accuracy of more than three orders of magnitude with respect to previously available data.[100] The ^{86}Sr optical frequency then amounts to 434 828 957 494 (10) kHz.

8. Conclusions

The strontium atom is an attractive candidate both for physical studies and for applications. We have shown how the properties of atomic strontium are suited for laser cooling and trapping, for the study of ultracold atomic physics, and for applications to optical frequency metrology or to micrometric force sensors.

Future work on ultracold strontium offers intriguing perspectives, including the possible realization of a nearly non-interacting Bose–Einstein condensate, the realization of an optical clock with ultimate stability, or direct experimental tests of theories beyond the standard model.

Appendix A. Experimental Setup

The typical experimental setup for Sr laser cooling and trapping basically includes a vacuum system, a blue laser source for the atom collection and first cooling stage, a red laser for second stage cooling and precision spectroscopy, and an infrared laser

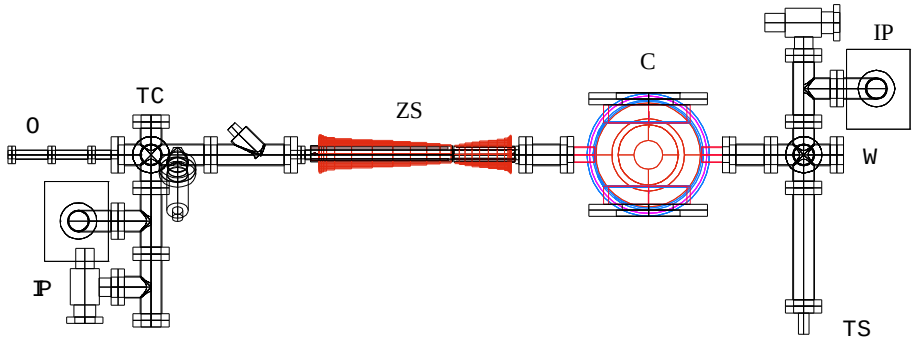

Fig. 16. Vacuum aparatus. O: oven for St sublimation; IP: ion pumps; TC: cell for transverse cooling; ZS: differential pumping tube for the Zeeman slower; C: MOT cell; TS: titanium sublimation pump; W: sapphire window for the Zeeman slower laser beam.

source for the optical dipole trap. In the following we illustrate these main parts as they are realized in our laboratory.

A.1. *Vacuum system*

The apparatus consists in three major parts: the oven, the Zeeman slower, and the MOT chamber. The oven generates an atomic strontium vapor by sublimation from metallic strontium kept at $\sim$ 800 Kelvin. The vapor is collimated into an atomic beam passing through a nozzle filled with about 200 stainless steel capillaries 8 mm long which insure a ballistic divergence of the atomic beam of 20 mRad.[101] Keeping the capillaries at a higher temperature prevents internal vapor condensation and clogging.

Following the atomic trajectory (see the sketch in Fig. 16), the atoms pass through a region with radial optical access for 2D transverse cooling,[30,31] they are decelerated through the Zeeman slower,[29] and finally stopped in the cell that hosts the MOT. The optical access for 2D transverse cooling is provided by a CF35 cube aligned on the atomic beam. On the two free direction two pairs of windows, AR coated for 461 and 689 nm, are sealed with modified copper gaskets.[102] A differential pumping stage between the transverse cooling region and the Zeeman slower insures decoupled background pressure between the oven and MOT region. The oven is pumped by a 20 l/s ion pump while the MOT is pumped by a 20 l/s ion pump and a titanium sublimation pump. With this setup, in operation condition, we achieve a pressure of 10^{-7} Torr in the transverse cooling region, and a pressure of 10^{-9} Torr on the MOT cell. A BK7 window on the atomic beam axis provides access for the Zeeman slower decelerating beam. To prevent chemical reaction of strontium and darkening, the anti-reflection is only present on the outer side of the window, and the window is heated to $\sim$ 450 Kelvin. Paying attention to block the Sr beam when unnecessary, the window presents a dim shadow after two years of operation. In the future we plan to exchange the window with a sapphire one,

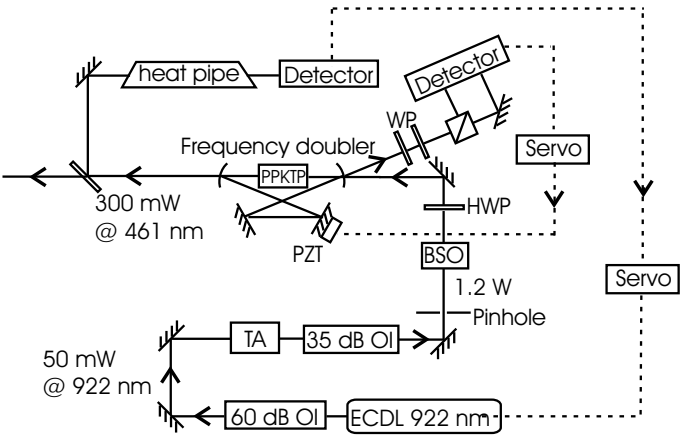

Fig. 17. Scheme of the laser at 461 nm. A distributed feedback laser (DFB) is amplified in a semiconductor tapered amplifier (TA), and frequency doubled on a periodically poled KTP crystal. The nonlinear conversion is improved by placing the KTP crystal into an optical resonator. Optical isolators (OI) between the DFB and TA, and between the TA and the frequency doubling stage. Solid lines represent the optical path, dashed lines represent electrical connections. BSO: beam shaping optics.

again anti-reflection coated on the outer side, from which deposited Sr can be easily removed.

A.2. *Blue laser sources*

The light at 461 nm (see Fig. 1) used for the atomic beam deceleration and capture in the MOT is produced by second-harmonic generation (SHG) of a 922 nm semiconductor laser (see Fig. 17). We generate the 922 nm radiation with a master oscillator-parametric amplifier system (MOPA). An anti-reflection coated laser diode mounted in an extended cavity in Littrow configuration (ECDL)[103] delivers 50 mW at 922 nm, that is amplified to 1.2 W in a tapered amplifier (TA). Optical isolators are placed between the ECDL and the TA, and between the TA and the frequency doubler cavity, in order to prevent optical feedback into the master laser, and optical damages on the amplifier. The frequency doubler is composed of a 20 mm long periodically-poled KTP crystal, placed in an optical build up cavity. The crystal facets are anti-reflection coated both at 922 and 461 nm ($R < 0.2\%$) and the poling period is chosen to fulfill quasi-phase matching of our wavelength at room temperature. The resonator has an input coupling mirror with 11% transmission and it is held in resonance with the input light feeding the error signal from a Hänsch–Couillaud detector[104] to a PZT controlled folding mirror. Under optimal conditions we obtain 300 mW in the blue and routinely we work with 200 mW. We frequency stabilize this blue source to the $^1S_0$-$^1P_1$ line of ^{88}Sr by means of conventional saturated spectroscopy in a strontium heatpipe. The servo loop acts on the piezo of the ECDL.

The light used for atomic manipulation and detection is brought to the vacuum system through single-mode polarization-maintaining optical fibers to improve the long-term beam pointing stability.

As we discussed in Sec. 3.3, we employ a turquoise laser at 497 nm to increase the MOT lifetime and number of atoms loaded. As in the case of 461 nm source, there are no laser diodes available at 497 nm and the simplest method to produce this light is frequency doubling an IR laser at 994 nm. In this application 1 mW of light is sufficient to saturate the process, then we do not need any amplification of the IR light before frequency doubling. The source at 497 nm differs from that at 461 nm in few parts. The master laser is an anti-reflection coated diode in ECDL Littrow configuration. After the beam shaping optics, the IR light is coupled into a bow-tie cavity that contains a 17 mm long, b-cut potassium niobate crystal which is kept at 328 K in order to satisfy non-critical phase matching for SHG. The crystal facets are AR coated both for the fundamental and the blue light and, like the 461 nm source, the cavity is kept resonant to the 994 nm laser with a Hänsch–Couillaud locking. Since this laser operates among Sr excited states it is not possible to lock the laser to the atomic line on a simple heatpipe. Possible frequency stabilization methods include locking to a reference cavity or spectroscopy on an atomic sample with a suitable fraction of excited atoms, such as a hollow cathode lamp, or an heatpipe with gas discharge, or simply the MOT. We chose the latter system, in spite of the fact that the blue MOT fluorescence signal is not continuously available during our measurement cycles. In fact the short-term laser frequency stability is sufficient to keep it in resonance with the $^3P_2$-$^3D_2$ transition for some tens of seconds. Thus we leave the laser free running, and we manually adjust its frequency at the beginning of the measurement cycle by acting on the piezo of the ECDL to maximize the MOT fluorescence.

A.3. *Red laser source*

The 689 nm source is composed of a laser diode frequency-locked to an optical cavity whose modes are stabilized to keep the laser on resonance with the atomic line. A scheme of the experimental setup is given in Fig. 18. An extended cavity laser-diode mounted in the Littrow configuration delivers 15 mW at 689 nm. Optical feedback into the ECDL is prevented by a 40 dB optical isolator and a single pass acusto-optic modulator in cascade. The laser linewidth is reduced by locking the laser to an optical reference cavity (RC) with standard Pound–Drever–Hall technique;[105] the phase modulation is produced by an electro-optic modulator (EOM) driven at 11 MHz and leaves 85% of the power in the carrier. The reference cavity has a free spectral range (FSR) of 1.5 GHz and a finesse of ~ 7000. On one side of the quartz spacer we glued a concave mirror ($R = 50$ cm) while on the other side a PZT is glued between the spacer and a flat mirror in order to steer the modes of the cavity by more than one FSR.

The locking loop includes a low frequency channel acting on the PZT of the

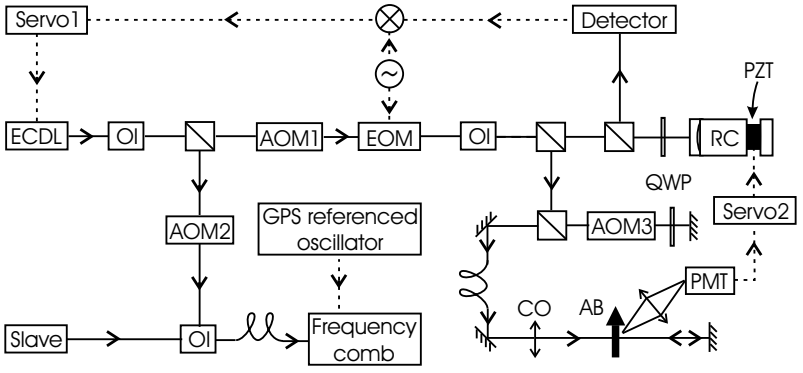

Fig. 18. Scheme of the 689 nm laser. Experimental setup used for the frequency measurement on the Sr intercombination line. Optical isolators (OI) and acusto-optic modulators (AOM) eliminate feedback among the master laser (ECDL), the slave laser, the electro-optic modulator (EOM) and the reference cavity (RC). QWP: quarter wave-plate. CO: collimation optics. PMF: polarization maintaining fiber. PMT: photo multiplier tube. The same apparatus is used for Sr second stage cooling and trapping, but the thermal beam is replaced by an heat-pipe.

ECDL (1 kHz bandwidth), and a high frequency channel acting on the laser-diode current supply (~ 3 MHz bandwidth). Under lock condition more than 55% of the incident light is transmitted through the cavity. From the frequency noise spectrum obtained by comparison with an independent cavity we can infer a laser linewidth lower than 20 Hz, and more than 90% of the optical power in the carrier.[106,107] The RC is acoustically isolated, though we do not keep it under vacuum.[108] The optical table is actively isolated from seismic noise with pneumatic legs. The frequency drifts of the cavity are compensated by the servo to the atomic signal which acts on the PZT of the high finesse cavity with a 20 Hz bandwidth. In the frequency measurement experiment described in Sec. 7.1, the Doppler free saturated fluorescence on a thermal strontium beam provides the signal for cavity stabilization on the atomic line. The thermal beam source has a similar design as described in Appendix A.1 and it is pumped by a 20 l/s ion pump. However, when using the stable 689 nm laser for second stage cooling and trapping, as described in Sec. 3.4, we employ an heat-pipe kept at ~ 750 K instead of the thermal beam, thus obtaining a larger signal and a more robust lock.

A.4. *Infrared laser sources for dipole trapping*

After the production of an ultracold sample in double stage magneto-optical trapping, we transfer the atoms in an optical dipole trap made of two infrared laser beams crossing each other near the waist. The two beams, respectively aligned along the horizontal and vertical direction, are produced with two independent TA injected with light coming from the same infrared source used for producing the blue light (see Fig. 19), that is close enough to the "magic wavelength" for the $^1S_0$-$^3P_1$ transition. Typically 300 mW of light coming from that source are

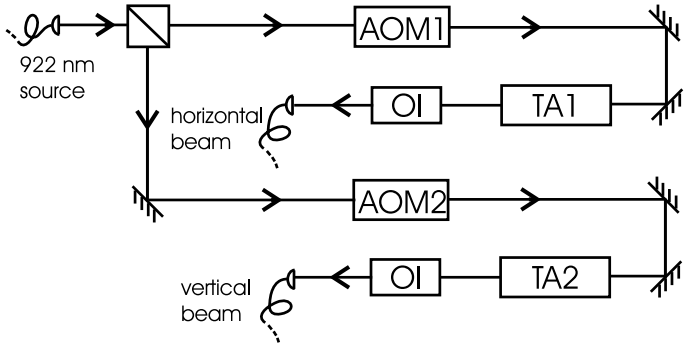

Fig. 19. The 922 nm laser source for the optical dipole trap.

coupled into a fiber and sent to the two amplifiers. The injection of the two TAs it is regulated by two AOMs which are used to shift the frequency of the two beams (avoiding interference at the center of the dipole trap) and to apply a fast control to the output TA optical power. For mode cleaning and delivering the output beams from the TAs to the atoms, we use two independent single mode fibers. Typically we obtain about 650 mW and 440 mW at the fiber output for the horizontal and vertical beams, respectively. We finally focus the beams at the MOT center, with $1/e^2$ radii of 15 μm and 35 μm respectively.

References

1. H. Katori, T. Ido, Y. Isoya and M. Kuwata-Gonokami, *Phys. Rev. Lett.* **82** (1999) 1116.
2. G. Ferrari, N. Poli, R. E. Drullinger, F. Sorrentino and G. Tino, *Phys. Rev. A* **73** (2006) 023408.
3. T. Mukaiyama, H. Katori, T. Ido, Y. Li and M. Kuwata-Gonokami, *Phys. Rev. Lett.* **90** (2003) 113002.
4. X. Xu, T. H. Loftus, J. W. Dunn, C. H. Greene, J. L. Hall, A. Gallagher and J. Ye, *Phys. Rev. Lett.* **90** (2003) 193002.
5. T. H. Loftus, T. Ido, A. D. Ludlow, M. M. Boyd and J. Ye, *Phys. Rev. Lett.* **93** (2004) 073003.
6. H. Katori, T. Ido, Y. Isoya and M. Kuwata-Gonokami, in *Atomic Physics*, Vol. 17, eds. E. Arimondo, P. De Natale and M. Inguscio (AIP, New York, 2001), p. 382.
7. M. Takamoto and H. Katori, *Phys. Rev. Lett.* **91** (2003) 223001.
8. I. Courtillot, A. Quessada, R. P. Kovacich, A. Brusch, D. Kolker, J.-J. Zondy, G. D. Rovera and P. Lemonde, *Phys. Rev. A* **68** (2003) 030501(R).
9. G. Ferrari, P. Cancio, R. Drullinger, G. Giusfredi, N. Poli, M. Prevedelli, C. Toninelli and G. M. Tino, *Phys. Rev. Lett.* **91** (2003) 243002.
10. T. Ido, T. H. Loftus, M. M. Boyd, A. D. Ludlow, K. W. Holman and J. Ye, *Phys. Rev. Lett.* **94** (2005) 153001.
11. Y. Bidel, B. Klappauf, J. C. Bernard, D. Delande, G. Labeyrie, C. Miniatura, D. Wilkowski and R. Kaiser, *Phys. Rev. Lett.* **88** (2002) 203902.
12. A. Derevianko, S. G. Porsev, S. Kotochigova, E. Tiesinga and P. S. Julienne, *Phys. Rev. Lett.* **90** (2003) 063002.

13. E. L. Raab, M. Prentiss, A. Cable, S. Chu and D. Pritchard, *Phys. Rev. Lett.* **59** (1987) 2631.
14. T. Kurosu and F. Shimizu, *Jpn. J. Appl. Phys.* **29** (1990) L2127.
15. T. Chaneliére, D. Wilkowski, Y. Bidel, R. Kaiser and C. Miniatura, *Phys. Rev. E* **70** (2004) 036602.
16. G. Ferrari, N. Poli, F. Sorrentino and G. Tino, *Phys. Rev. Lett.* **97** (2006) 060402.
17. H. Katori, T. Ido and M. K. Gonokami, *J. Phys. Soc. Jpn.* **68** (1999) 2479.
18. T. Ido, Y. Isoya and H. Katori, *Phys. Rev. A* **61** (2000) 061403.
19. M. Takamoto, F.-L. Hong, R. Higashi and H. Katori, *Nature* **435** (2005) 321.
20. T. Kishimoto, H. Hachisu, J. Fujiki, K. Nagato, M. Yasuda and H. Katori, *Phys. Rev. Lett.* **96** (2006) 123001.
21. P. Lemonde and P. Wolf, *Phys. Rev. A* **72** (2005) 033409.
22. R. Le Targat, X. Baillard, M. Fouché, A. Brusch, O. Tcherbakoff, G. D. Rovera and P. Lemonde (2006), arXiv:physics/0605200.
23. S. B. Nagel, P. G. Mickelson, A. D. Saenz, Y. N. Martinez, Y. C. Chen, T. C. Killian, P. Pellegrini and R. Côté, *Phys. Rev. Lett.* **94** (2005) 083004.
24. P. G. Mickelson, Y. N. Martinez, A. D. Saenz, S. B. Nagel, Y. C. Chen, T. C. Killian, P. Pellegrini and R. Côté, *Phys. Rev. Lett.* **95** (2005) 223002.
25. T. Chaneliére, J.-L. Meunier, R. Kaiser, C. Miniatura and D. Wilkowski (2004), arXiv:physics/0412119v1.
26. A. Corney, *Atomic and Laser Spectroscopy* (Clarendon Press, Oxford, New York, 1977).
27. J. Grünert and A. Hemmerich, *Phys. Rev. A* **65** (2002) 041401.
28. C. W. Oates, F. Bondu and L. Hollberg, *Eur. Phys. J. D* **7** (1999) 449.
29. J. V. Prodan, W. D. Phillips and H. Metcalf, *Phys. Rev. Lett.* **49** (1982) 1149.
30. F. Shimizu, K. Shimizu and H. Takuma, *Chem. Phys.* **145** (1990) 327.
31. E. Rasel, F. Pereira Dos Santos, F. S. Pavone, F. Perales, C. S. Unnikrishnan and M. Leduc, *Eur. Phys. J. D* **7** (1999) 311.
32. T. P. Dinnen, K. R. Vogel, E. Arimondo, J. L. Hall and A. Gallagher, *Phys. Rev. A* **59** (1999) 1216.
33. T. Mukaiyama, H. Katori, T. Ido, Y. Li and M. Kuwata-Gonokami, *Phys. Rev. Lett.* **90** (2003) 113002.
34. T. Binnewies, G. Wilpers, U. Sterr, F. Rihele, J. Helmke, T. E. Mehlstäubler, E. M. Rasel and W. Ertmer, *Phys. Rev. Lett.* **87** (2001) 123002.
35. M. S. Santos, P. Nussenzveig, L. G. Marcassa, K. Helmerson, J. Flemming, S. C. Zilio and V. S. Bagnato, *Phys. Rev. A* **52** (1995) R4340.
36. M. Murdrich, S. Kraft, K. Singer, R. Grimm, A. Mosk and M. Weidemüller, *Phys. Rev. Lett.* **88** (2002) 253001.
37. R. J. W. Stas, J. M. McNamara, W. Hogervorst and W. Vassen, *Phys. Rev. Lett.* **93** (2004) 053001.
38. T. Loftus, J. R. Bochinski and T. W. Mossberg, *Phys. Rev. A* **63** (2001) 053401.
39. K. Honda, Y. Takasu, T. Kuwamoto, M. Kumakura, Y. Takahashi and T. Yabuzaki, *Phys. Rev. A* **66** (2002) 021401(R).
40. M.-O. Mewes, G. Ferrari, F. Schreck, A. Sinatra and C. Salomon, *Phys. Rev. A* **61** (1999) 011403(R).
41. F. Schreck, G. Ferrari, K. L. Corwin, J. Cubizolles, L. Khaykovich, M.-O. Mewes and C. Salomon, *Phys. Rev. A* **64** (2001) 011402.
42. F. Schreck, L. Khaykovich, K. L. Corwin, G. Ferrari, T. Bourdel, J. Cubizolles and C. Salomon, *Phys. Rev. Lett.* **87** (2001) 080403.

43. W. Suptitz, G. Wokurka, F. Strauch, P. Kohns and W. Ertmer, *Opt. Lett.* **19** (1994) 1571.
44. J. Stuhler, P. O. Schmidt, S. Hensler, J. Werner, J. Mlynek and T. Pfau, *Phys. Rev. A* **64** (2001) 031405(R).
45. S. B. Nagel, C. E. Simien, S. Laha, P. Gupta, V. S. Ashoka and T. C. Killian, *Phys. Rev. A* **67** (2003) 011401(R).
46. N. Poli, R. E. Drullinger, G. Ferrari, J. Léonard, F. Sorrentino and G. Tino, *Phys. Rev. A* **71** (2005) 061403(R).
47. R. Grimm, M. Weidemüller and Y. B. Ovchinnikov, *Adv. At. Mol. Opt. Phys.* **42** (2000) 95.
48. R. H. Dicke, *Phys. Rev.* **89** (1953) 472.
49. T. Ido and H. Katori, *Phys. Rev. Lett.* **91** (2003) 053001.
50. P. O. Fedichev, M. W. Reynolds and G. V. Shlyapnikov, *Phys. Rev. Lett.* **77** (1996) 2921.
51. G. Delannoy, S. G. Murdoch, V. Boyer, V. Jossel, P. Bouyer and A. Aspect, *Phys. Rev. A* **63** (2001) 051602(R).
52. M. Yamashita and T. Mukai, *Phys. Rev. A* **68** (2003) 063601.
53. Tc. R. Monroe, E. A. Cornell, C. A. Sackett, C. J. Myatt and C. E. Wieman, *Phys. Rev. Lett.* **70** (1993) 414.
54. M. Arndt, M. Ben Dahan, D. Guéry-Odelin, M. W. Reynolds and J. Dalibard, *Phys. Rev. Lett.* **79** (1997) 625.
55. S. A. Hopkins, S. Webster, J. Arlt, P. Bance, S. Cornish, O. Marago and C. J. Foot, *Phys. Rev. A* **61** (2000) 032707-1.
56. P. O. Schmidt, S. Hensler, J. Werner, A. Griesmaier, A. Görlitz, T. Pfau and A. Simoni, *Phys. Rev. Lett.* **91** (2003) 193201.
57. S. D. Gensemer and D. S. Jin, *Phys. Rev. Lett.* **87** (2001) 173201.
58. D. Guéry-Odelin, F. Zabelli, J. Dalibard and S. Stringari, *Phys. Rev. A* **60** (1999) 4851.
59. G. M. Kavoulakis, C. J. Pethick and H. Smith, *Phys. Rev. A* **61** (2000) 053603.
60. M. Yasuda, T. Kishimoto, M. Takamoto and H. Katori, *Phys. Rev. A* **73** (2006) 011403(R).
61. J. Goldwin, S. Inouye, M. L. Olsen, B. Newman, B. D. DePaola and D. S. Jin, *Phys. Rev. A* **70** (2004) 021601.
62. G. Ferrari, M. Inguscio, W. Jastrzebski, G. Modugno, G. Roati and A. Simoni, *Phys. Rev. Lett.* **89** (2002) 053202.
63. A. Mosk, S. Kraft, M. Murdrich, K. Singer, W. Wohlleben, R. Grimm and M. Weidemüller, *Appl. Phys. B* **73** (2004) 791.
64. G. Delannoy, S. G. Murdoch, V. Boyer, V. Josse, P. Bouyer and A. Aspect, *Phys. Rev A* **63** (2001) 051602(R).
65. E. A. Burt, R. W. Ghrist, C. J. Myatt, M. J. Holland, E. A. Cornell and C. E. Wieman, *Phys. Rev. Lett.* **79** (1997) 337.
66. H. F. Hess, *Phys. Rev. B* **34** (1986) (R)3476.
67. Y. Takasu, K. Maki, K. Komori, T. Takano, K. Honda, M. Kumakura, T. Yabuzaki and Y. Takahashi, *Phys. Rev. Lett.* **91** (2003) 040404.
68. T. Weber, J. Herbig, M. Mark, H.-C. Naegerl and R. Grimm, *Science* **299** (2002) 232.
69. T. Kinoshita, T. Wenger and D. S. Weiss, *Phys. Rev. A* **71** (2005) 011602(R).
70. A. Peters, K. Y. Chung and S. Chu, *Nature* **400** (1999) 849.
71. T. L. Gustavson, A. Landragin and M. A. Kasevich, *Class. Quantum Grav.* **17** (2000) 2385.

72. A. Wicht, J. M. Hensley, E. Sarajlic and S. Chu, *Physica Scripta* **102** (2002) 82.
73. P. Cladé, E. de Mirandes, M. Cadoret, S. Guellati-Khélifa, C. Schwob, F. Nez, L. Julien and F. Biraben, *Phys. Rev. Lett.* **96** (2006) 033001.
74. J. Stuhler, M. Fattori, T. Petelski and G. M. Tino, *J. Opt. B: Quantum Semiclass. Opt.* **5** (2003) S75.
75. S. Fray, C. A. Diez, T. W. Hänsch and M. Weitz, *Phys. Rev. Lett.* **93** (2004) 240404.
76. M. Antezza, L. P. Pitaevskii and S. Stringari, *Phys. Rev. Lett.* **95** (2005) 113202.
77. J. C. Long, H. W. Chan, A. B. Churnside, E. A. Gulbis, M. C. M. Varney and J. C. Price, *Nature* **421** (2003).
78. S. Dimopoulos and A. A. Geraci, *Phys. Rev. D* **68** (2003) 124021.
79. S. J. Samullin, A. A. Geraci, D. M. Weld, J. Chiaverini, S. Holmes and A. Kapitulnik, *Phys. Rev. D* **72** (2005) 122001.
80. I. Bloch, *Nature Physics* **1** (2005) 23.
81. F. Bloch, *Z. Phys.* **52**, 555 (1929).
82. M. Raizen, C. Salomon and Q. Niu, *Physics Today* **50**(7) (1997) 30.
83. B. P. Anderson and M. A. Kasevich, *Science* **282** (1998) 1686.
84. G. Roati, E. de Mirandes, F. Ferlaino, H. Ott, G. Modugno and M. Inguscio, *Phys. Rev. Lett.* **92** (2004) 230402.
85. Th. Udem, J. Reichert, R. Holzwarth and T. W. Hänsch, *Opt. Lett.* **24** (1999) 881.
86. S. A. Diddams, D. J. Jones, J. Ye, S. T. Cundiff, J. L. Hall, J. K. Ranka, R. S. Windeler, R. Holzwarth, T. Udem and T. W. Hänsch, *Phys. Rev. Lett.* **84** (2000) 5102.
87. Th. Udem, R. Holzwarth and T. W. Hänsch, *Nature* (*London*) **416** (2002) 233.
88. T. Udem, S. A. Diddams, K. R. Vogel, C. W. Oates, E. A. Curtis, W. D. Lee, W. M. Itano, R. E. Drullinger, J. C. Bergquist and L. Hollberg, *Phys. Rev. Lett.* **86** (2001) 4996 and references therein.
89. P. Gill, *Metrologia* **42** (2005) S125.
90. H. Katori, M. Takamoto, V. G. Pal'chikov and V. D. Ovsiannikov, *Phys. Rev. Lett.* **91** (2003) 173005.
91. J. L. Hall, M. Zhu and P. Buch, *J. Opt. Soc. Am. B* **6** (1989) 2194.
92. G. M. Tino, M. Barsanti, M. de Angelis, L. Gianfrani and M. Inguscio, *Appl. Phys. B* **55** (1992) 397.
93. A. Ludlow, M. M. Boyd, T. Zelevinsky, S. M Foreman, S. Blatt, M. Notcutt, T. Ido and J. Ye, arXiv:physics/0508041 (2005).
94. C. W. Hoyt, Z. W. Barber, C. W. Oates, T. M. Fortier, S. A. Diddams and L. Hollberg (2005), arXiv:physics/0503240.
95. R. Santra, E. Arimondo, T. Ido, C. H. Greene and J. Ye, *Phys. Rev. Lett.* **94** (2005) 173002.
96. T. Hong, C. Cramer, E. Cook, W. Naugourney and E. N. Fortson, *Phys. Rev. Lett.* **94** (2005) 050801.
97. A. V. Taichenachev, V. I. Yudin, C. W. Oates, C. W. Hoyt, Z. W. Barber and L. Hollberg, *Phys. Rev. Lett.* **96** (2006) 083001.
98. Z. W. Barber, C. W. Hoyt, C. W. Oates, L. Hollberg, A. V. Taichenachev and V. I. Yudin, *Phys. Rev. Lett.* **96** (2006) 083002.
99. S. T. Cundiff, J. Ye and J. L. Hall, *Rev. Sci. Instr.* **72** (2001) 3749.
100. F. Buchinger, R. Corriveau, E. B. Ramsay, D. Berdichevsky and D. W. L. Sprung, *Phys. Rev. C* **32** (1985) 2058.
101. I. Courtillot, A. Quessada, R. P. Kovacich, J. J. Zondy, A. Landragin, A. Clairon and P. Lemonde, *Opt. Lett.* **28** (2003) 468.
102. A. Noble and M. Kasevich, *Rev. Sci. Instr.* **65** (1994) 3042.

103. C. E. Wieman and L. Hollberg, *Rev. Sci. Instr.* **62** (1991) 1.
104. B. Couillaud and T. W. Hänsch, *Opt. Comm.* **35** (1981) 441.
105. R. W. P. Drever, J. L. Hall, F. V. Kowalski, J. Hough, G. M. Ford, A. J. Munley and H. Ward, *App. Phys B* **31** (1983) 97.
106. G. Ferrari, T. Brzozowski, R. E. Drullinger, N. Poli, M. Prevedelli, C. Toninelli and G. M. Tino, *Proc. SPIE* **5478** (2004) 5.3.
107. N. Poli, G. Ferrari, M. Prevedelli, F. Sorrentino, R. E. Drullinger and G. M. Tino, *Spectrochim. Acta Part A* **63** (2006) 981.
108. B. C. Young, F. C. Cruz, W. M. Itano and J. C. Bergquist, *Phys. Rev. Lett.* **82** (1999) 3799.
109. J. A. Neuman, P. Wang and A. Gallagher, *Rev. Sci. Instrum.* **66** (1995) 3021.
110. G. Modugno, G. Ferrari, G. Roati, R. J. Brecha, A. Simoni and M. Inguscio, *Science* **294** (2001) 1320.